Available online at www.sciencedirect.com
ScienceDirect
Journal of Sound and Vibration 298 (2006) 12–29
JOURNAL OF SOUND AND VIBRATION
www.elsevier.com/locate/jsvi

A theoretical analysis in the time-domain of wave reflection on a bone plate

Quentin Grimal[a], Salah Naïli[b,*]

[a]*Laboratoire d'Imageric Paramétrique, CNRS UMR 7623, Université Pierre et marie Curie, 15 rue de l'école de médecine, 75006 Paris France*

[b]*Laboratoire de Mécanique Physique, CNRS UMR 7052 B20A, Faculté des Sciences et Technologie, Université Paris XII-Val de Marne, 61, Avenue du Général de Gaulle, 94010 Créteil Cédex, France*

Received 13 December 2004; received in revised form 16 January 2006; accepted 10 April 2006
Available online 7 July 2006

Abstract

This paper presents an original method for simulating ultrasonic wave reflection on a fluid-loaded plate. Geometrical and material parameters used are relevant to the "axial transmission technique" (ATT) setup. Devices based on the ATT are used for the assessment of cortical bone strength (estimate of a fracture risk). In this work, the cortical bone layer is represented as a plate of infinite extent surrounded by fluid (soft tissues). A line source and a receiver are placed in the fluid. Transient waves generated upon reflection at the plate–fluid interfaces are addressed. Analytic Green's functions are derived with the generalized ray/Cagniard-de Hoop method. The acoustic response is obtained upon convolution of Green's functions with a given source pulse. The method associates each wave amplitude in the time-domain (lateral waves, reflected body waves, etc.) to a specific term of the final solution. The method is ideally suited to a detailed analysis of the ultrasonic signal for various geometrical and mechanical parameters. The results presented highlight the potential of the method for the understanding of wave phenomena involved in the ATT and similar setups. They also bring new elements that reinforce our theoretical knowledge of the ATT.

1. Introduction

Low bone mechanical strength increases the risk of having a fracture under minimal trauma such as falls in daily life (low energy fractures). The rate of incidence of minimal trauma fractures is high in postmenopausal women and expected to increase with the aging of the population; osteoporosis is one cause of the decrease of bone strength. Fractures cause disability, which in some cases leads to death, and generates important health care costs [1]. Hence it is a major public health concern to identify those individuals with low bone mechanical properties so that preventive and/or therapeutic measures can be instituted.

The reference methods for the assessment of bone fragility are based on measurements of X-ray attenuation. These techniques quantifies the amount of bone mineral, which is used for estimating bone strength *in vivo* and the risk of minimal trauma fracture [1]. The definition of osteoporosis is presently based on measurements

*Corresponding author. Tel.: +33 1 45 17 14 45; fax: +33 1 45 17 14 33.
E-mail addresses: quentin.grimal@upmc.fr (Q. Grimal), naili@univ-paris12.fr (S. Naïli).

0022-460X/$ - see front matter © 2006 Elsevier Ltd. All rights reserved.
doi:10.1016/j.jsv.2006.04.037

with the dual energy X-ray absorptiometry (DXA) technique which integrates the mass of bone mineral and the bone size. However, only 60–70% of the bone resistance to fracture—as determined *in vitro* on isolated skeletal pieces—is correlated to the amount of bone mineral [2]: bone strength depends not only on bone mass but also on bone geometry, microarchitecture, fatigue damage and bone tissues intrinsic mechanical properties. X-ray methods are widely used and have proved some efficiency; however, they only give access to mechanical properties in an indirect way. Other drawbacks of X-ray techniques is their cost and in some situations the limitations in terms of X-ray radiation exposure.

Ultrasonic measurements are an alternative to X-ray-based methods. The ultrasonic signal is based on a mechanical phenomenon—the interaction of elastic waves with matter—and conveys much information related to the mechanical properties of bone tissue. At present, devices based on ultrasound propagation and used for clinical purposes yield an estimate of the speed of sound in bone and an estimate of the ultrasonic signal attenuation. Further research on the interaction of ultrasound waves with bone seems necessary because: (i) other mechanics-related parameters than speed of sound and attenuation are expected to be relevant for improving diagnosis (e.g. elastic parameters); (ii) the design and utilization of existing clinical devices could be improved based on a better understanding of wave phenomena.

The present study is a contribution to the understanding of wave phenomena involved in the ultrasonic "axial transmission technique" (ATT) for the evaluation of bone. A schematic illustration of the technique is given in Fig. 1. Devices based on the ATT are used to investigate the cortical layer of long bones for the diagnosis of osteoporosis [3–5]. In a typical axial transmission experiment, the cortical layer is excited by a ultrasonic pulse with center frequency between 0.5 and 2 MHz [6,7]; a value of a "wave speed" in the cortical bone is deduced from the arrival time of the first signal arrived at the receiver. Clearly, the interpretation of the estimated "wave speed", in terms of material properties of bone, depends on the wave path associated with the first arriving signal. The estimated value for the wave speed is very sensitive to material and geometrical parameters of bone on the one hand [7] and to the center frequency of the pulse used by the device, on the other hand [8].

The main purpose of this paper is to present an original method for simulating wave propagation in a model representing the setup of the ATT. The first results obtained with the method are shown; they bring new elements that reinforce the theoretical basis needed for the analysis of the ultrasonic signal generated with the ATT. The general idea of the work is (i) to help interpret the wave signals obtained from current and future devices based on the ATT; (ii) to help determine which mechanical parameters could possibly be measured with the ATT, based on the sensitivity of the wave amplitudes and arrival times to the variations of these parameters within the physiological range.

A two-dimensional (2D) idealized model of the ATT setup is considered: two semi-infinite ideal fluid media (representing soft tissues) and a plate of infinite extent (representing the cortical bone layer), see Fig. 2. A line source of pressure and a receiver are placed in the fluid medium. With this simple geometrical configuration, the relative importance of some parameters governing the interaction of ultrasound waves with the cortical layer should show up as clearly as possible.

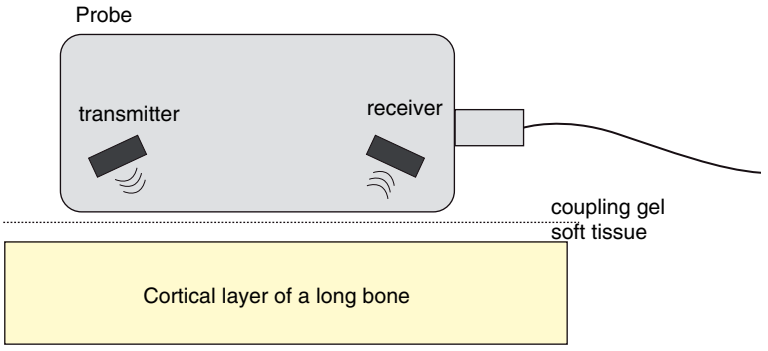

Fig. 1. Schematic illustration of a typical device used for measurements with the axial transmission technique. The length of the probe is 2–5 cm.

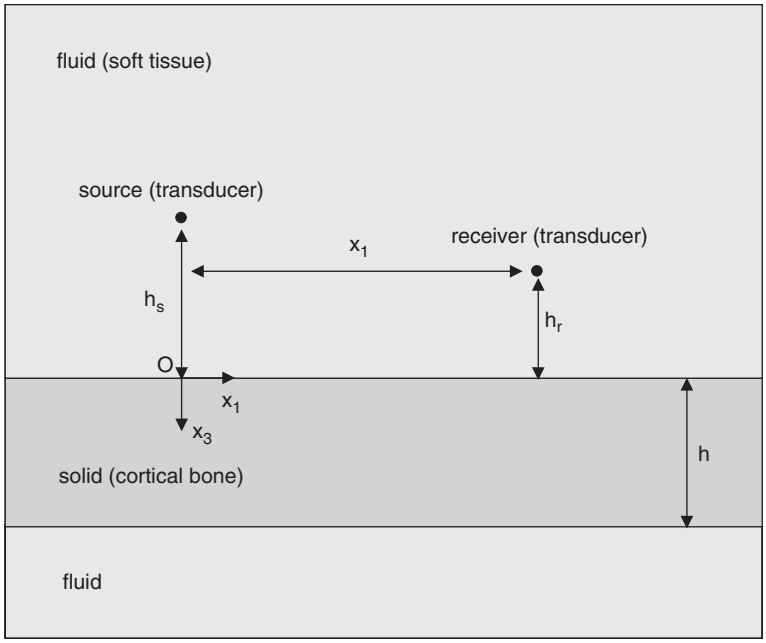

Fig. 2. Model geometry and coordinate system.

Some of the wave phenomena involved in the ATT have been addressed in Refs. [6,7] using a similar model configuration and with the help of numerical simulation based on the finite difference method. Results shown in Ref. [9] suggest that 2D modeling of the ATT experiment addresses the main physical phenomena. For the present study, an analytical method of solution based on the Cagniard–de Hoop technique was used instead. This technique has been developed to solve problems of transient wave propagation in layered media [10–13]. In the present paper, the application of the method to a fluid-loaded plate configuration is reported for the first time, as far as we know.

The main advantage of the analytical method used is that it yields Green's functions of the problem; the response to a given excitation pulse is then obtained by convolution of the pulse with the Green's function. The Green's functions reveal all the wave phenomena irrespective of an excitation pulse—depending on the duration and frequency content of an excitation pulse, a given phenomenon will show up or not in the convolved response. Furthermore, Green's functions are obtained for each waves, i.e., the various contributions to the wave field can be distinguished and analyzed separately. The Cagniard–de Hoop method yields exact Green's functions, i.e., valid in near field as well as in far field, in a semi-explicit (in some cases, explicit) form so that accurate numerical responses can be calculated rapidly (a few seconds on a standard computer). As far as we know, the method proposed gives the algebraic solution in the most detailed form possible. Note that Green's functions for the present problem could also have been derived using a method developed recently by Tadeu and António [14]. It is not the purpose of this paper to give a detailed presentation of the Cagniard-de Hoop method. In the following, we expose the main lines of the method and highlight its potential for the type of engineering application considered.

The present paper is organized as follows: after this introduction as background, Section 2 gives a description of the configuration and a formulation of the basic equations. The method of solution is presented in Sections 3 and 4: first, the solution is obtained in a Laplace–Fourier domain with the help of the generalized ray theory; second, the transformation back to the space-time domain is performed with the Cagniard–de Hoop technique. Some details on the implementation of the solutions and the evaluation of the acoustic pressure at a receiver are given in Section 5. Section 6 is dedicated to numerical results. In the last section, the potential use of the work in the context of the evaluation of bone mechanical properties by ultrasonic methods is discussed.

2. Formulation of the problem

2.1. Configuration and definitions

The model geometry is shown in Fig. 2. It consists in an infinite elastic plate immersed in an ideal fluid. The position is specified through the coordinates (x_1, x_2, x_3) with respect to a Cartesian reference frame $\mathbf{R}(O; \mathbf{x}_1, \mathbf{x}_2, \mathbf{x}_3)$ where O is the origin and $(\mathbf{x}_1, \mathbf{x}_2, \mathbf{x}_3)$ is an orthonormal basis for the space; the $\mathbf{x}_3$-axis is taken perpendicular to the fluid–solid interface. The fluid occupies the half-spaces $x_3 < 0$ and $x_3 > h$.

The fluid and the solid are at rest for $t < 0$. At $t = 0$, a cylindrical acoustic wave is generated in the fluid by a line source parallel to $(O; \mathbf{x}_2)$, placed at a distance h_s from the fluid-solid interface. As a consequence of the problem symmetry, all quantities are independent of x_2; hence in what follows the analysis is conducted in the plane $(O; \mathbf{x}_1, \mathbf{x}_3)$; in the rest of the paper, the coordinate x_2 is implicit when omitted in mathematical expressions. In the following, the wave field is calculated at a receiver placed in the fluid, at a distance h_r from the interface. The distance along the interface between the source and the receiver is x_1. In the paper, the surface $x_3 = 0$ will be referred to as the "fluid–solid interface", and the surface $x_3 = h$ will be referred to as "bottom surface".

The fluid and the solid are isotropic and have linearly elastic constitutive laws: the inverse of the fluid compressibility, denoted by K, is used to characterize the fluid and the Lamé constants λ and μ are used to characterize the solid. The mass density is denoted by ρ_f in the fluid and by ρ_s in the solid. The elastic wave motion will be characterized in $\mathbf{R}$ by the particle velocity $\mathbf{v}$ and by the acoustic pressure p (in the fluid) or the components σ_{ij} of the Cauchy stress tensor (in the solid). The fluid flow is disregarded.

The wave speed in the fluid is defined by $c_f = \sqrt{K/\rho_f}$ and the wave slowness by $s_f = 1/c_f$. In the solid, letters P and S are associated with longitudinal waves and transverse waves polarized in the direction $\mathbf{x}_3$, respectively. Due to the nature of the source and the geometrical configuration, transverse waves polarized in the $(\mathbf{x}_1, \mathbf{x}_2)$ plane are not excited. Wave speeds in the solid are defined by $c_P = \sqrt{(\lambda + 2\mu)/\rho_s}$ and $c_S = \sqrt{\mu/\rho_s}$, and waves slownesses by $s_{P,S} = 1/c_{P,S}$. All through the paper, each time a comma appears between P and S means that the quantities relative to P- or S-waves, respectively, must be used.

2.2. Governing equations, boundary and initial conditions

2.2.1. Equations in the fluid

In order to describe the wave motion in the fluid, the equation of motion and the constitutive equation are taken in the form [15] (p. 44)

$$\partial_i p = -\rho_f \partial_t v_i, \quad i = 1, 3 \tag{1}$$

$$\partial_t p + K \partial_i v_i = K \phi_V(t) \delta(x_1) \delta(x_3 + h_s), \tag{2}$$

where the volume density of body forces is neglected in the equation of motion. The term on the right-hand side of Eq. (2) introduces a source of acoustic waves along a line parallel to $(O; \mathbf{x}_2)$, with history $\partial_t \phi_V(t)$. Einstein summation convention is used. Derivatives with respect to t and x_i are denoted ∂_t and ∂_i, respectively. The Dirac function is denoted $\delta(x)$.

2.2.2. Equations in the solid

The equation of motion in the solid is

$$\partial_j \sigma_{ij} - \rho \partial_t v_i = 0, \quad i, j = 1, 2, 3, \tag{3}$$

where the volume density of body forces is neglected. The constitutive equation (Hooke's law)

$$\sigma_{ij} = c_{ijkq} \frac{1}{2} (\partial_q u_k + \partial_k u_q), \tag{4}$$

where c_{ijkq} is the stiffness tensor of fourth order. In this paper, where only the case of an isotropic material is considered, the stiffness tensor takes the form

$$c_{ijkq} = \lambda\delta_{ij}\delta_{kq} + \mu(\delta_{ik}\delta_{jq} + \delta_{iq}\delta_{jk}),$$

where δ_{ij} is the Kronecker symbol.

2.2.3. Boundary conditions

At the interfaces between the fluid and the solid on planes $x_3 = 0$ and $x_3 = h$, the following conditions are assumed:

$$\begin{aligned} &[[v_3(x_1, x_3, t)]] = 0, \\ &\sigma_{33}(x_1, x_3, t) = -p(x_1, x_3, t), \quad \sigma_{13}(x_1, x_3, t) = \sigma_{23}(x_1, x_3, t) = 0, \end{aligned} \tag{5}$$

where [[ ]] denotes the jump of a quantity across the interface.

3. Solution in the transform domain

The equations given in Section 2.2 are subjected to a one-sided Laplace transform with respect to time. As an example, the space-time domain particle velocity $v_i(\mathbf{x}, t)$ is transformed to its space-Laplace domain counterpart $\hat{v}_i(\mathbf{x}, s)$ according to

$$\hat{v}_i(\mathbf{x}, s) = \int_0^\infty \exp(-st) v_i(\mathbf{x}, t)\,\mathrm{d}t,$$

where the Laplace parameter s is real and positive. Subsequently, a Fourier transformation with respect to x_1 is applied to the Laplace-transformed equations. The Fourier–Laplace domain counterpart or, shortly, the transform domain counterpart $\tilde{v}_j(k, x_3, s)$ of $\hat{v}_j(\mathbf{x}, s)$ is

$$\tilde{v}_i(k, x_3, s) = \int_{-\infty}^\infty \exp(\mathrm{i}skx_1)\hat{v}_i\,\mathrm{d}x_1 = \int_{-\infty}^\infty \exp(s\xi x_1)\hat{v}_i\,\mathrm{d}x_1,$$

where $k = -\mathrm{i}\xi$ is the real Fourier transform parameter. The inverse Fourier transformation is

$$\hat{v}_i(\mathbf{x}, s) = \frac{s}{2\pi}\int_{-\infty}^\infty \exp(-\mathrm{i}skx_1)\tilde{v}_i\,\mathrm{d}k = \frac{s}{2\mathrm{i}\pi}\int_{-i\infty}^{i\infty} \exp(-s\xi x_1)\tilde{v}_i\,\mathrm{d}\xi.$$

3.1. Solution in a fluid of infinite extent

The problem solution in the transform domain is arrived at through algebraic manipulations of the transformed governing equations, with the generalized ray/Cagniard-de Hoop method.

The method has been extensively described elsewhere [12,13,16]. In order to give the reader an overview of the procedure, the basic steps for the derivation of the solution are presented for a fluid of infinite extent, i.e., the fluid–solid interface in the configuration sketched in Fig. 2 is at an infinite distance from the source. The solution obtained in a fluid of infinite extent is the contribution of the direct wave in the configuration of Fig. 2.

In the fluid, the problem is solved for the velocity $\tilde{v}_3$ and the acoustic pressure $\tilde{p}$. A motion–pressure vector is defined as $\mathbf{b}_f = (\tilde{v}_3, \tilde{p})$. The transform domain counterparts of Eqs. (1) and (2) are manipulated and rewritten as a system of equations:

$$\partial_3\mathbf{b}_f = -sA_f\mathbf{b}_f + \mathbf{F}, \tag{6}$$

where $\mathbf{F} = (\tilde{\phi}_V\delta(x_3 + h_s), 0)^{\mathrm{T}}$ is a vector containing the source term and A_f is a 2×2 matrix defined by

$$A_f = \begin{pmatrix} 0 & \dfrac{1}{\rho_f}\left(s_f^2 - \xi^2\right) \\ \rho_f & 0 \end{pmatrix}.$$

The eigenvalues of A_f are $\mp\gamma_f$ where $\gamma_f = (s_f^2 - \xi^2)^{1/2}$. For the derivations to follow, it is necessary to restrict the values of ξ to a single sheet of the Riemann surface; the sheet where $\mathrm{Re}[\gamma_f] \geqslant 0$ is chosen (where Re[.] denotes the real part of the quantity between brackets)—this is equivalent to cutting the complex ξ-plane on the real axis along $]-\infty,\ s_f[$ and $]s_f,\ +\infty[$.

The eigenvalue matrix D_f is defined such that $D_f^{-1} A_f D_f$ is a diagonal matrix

$$D_f = \begin{pmatrix} -\dfrac{\gamma_f}{\rho_f} & \dfrac{\gamma_f}{\rho_f} \\ 1 & 1 \end{pmatrix},$$

and

$$D_f^{-1} = \begin{pmatrix} -\dfrac{\rho_f}{2\gamma_f} & \dfrac{1}{2} \\ \dfrac{\rho_f}{2\gamma_f} & \dfrac{1}{2} \end{pmatrix}.$$

Upon introducing $\mathbf{w}_f$ such that $\mathbf{b}_f = D_f \mathbf{w}_f$, Eq. (6) becomes

$$\partial_3 \mathbf{w}_f = -s \begin{pmatrix} -\gamma_f & 0 \\ 0 & \gamma_f \end{pmatrix} \mathbf{w}_f + \begin{pmatrix} \dfrac{-\rho_f \hat{\phi}_V}{2\gamma_f} \delta(x_3 + h_s) \\ \dfrac{\rho_f \hat{\phi}_V}{2\gamma_f} \delta(x_3 + h_s) \end{pmatrix}. \tag{7}$$

The homogeneous solution of Eq. (7) is

$$\mathbf{w}_f = \begin{pmatrix} W_- \exp(s\gamma_f x_3) \\ W_+ \exp(-s\gamma_f x_3) \end{pmatrix} = \begin{pmatrix} w_f^- \\ w_f^+ \end{pmatrix}. \tag{8}$$

where W_- and W_+ are determined from the boundary conditions at the source. Finally, the solution for the motion–pressure vector at a receiver at $h_r < h_s$ is

$$\mathbf{b}_f = \begin{pmatrix} \dfrac{\hat{\phi}_V}{2} \exp(-s\gamma_f(x_3 + h_s)) \\ \dfrac{\rho_f \hat{\phi}_V}{2\gamma_f} \exp(-s\gamma_f(x_3 + h_s)) \end{pmatrix}. \tag{9}$$

3.2. Wave contributions at the receiver

The motion–pressure vector corresponding to problem of wave reflection in the configuration sketched in Fig. 2 is derived with the generalized ray method. The method enables the construction of the wave field at the receiver in an intuitive manner. It has been shown elsewhere that a solution constructed this way is the exact solution of the problem [17,18] *in a prescribed time window*. A typical solution is a sum of several terms: the generalized rays; each term represents the contribution of a specific wave. Depending on the time window of interest, more or fewer wave contributions should be taken into account in the simulations; that is, the longer the time of observation, the more rays corresponding to waves multiply reflected on the surfaces of the plate should be calculated.

In the present study, the contributions due to the multiply reflected waves are not taken into account, i.e., only the short-time response is investigated; however, the construction of a solution which includes multiply reflected waves is straightforward with the method employed here. Three rays, or ray groups, are considered, referred to with symbols (D), (R) and $(R1)$:

- (D) the direct wave;
- (R) the wave reflected at the fluid-solid interface, referred to as the "reflected wave";

- ($R1$) longitudinal and transverse waves generated into the solid, reflected once on its bottom surface, and transmitted back to the fluid. This group is a collection of four contributions due to the conversion of waves. Waves of this group will be referred to as "waves reflected on the bottom surface".

Schematic ray paths corresponding to the three ray groups investigated are shown in Fig. 3. In the following we will use for various quantities an explicit subscript notation which indicates the geometrical ray path associated with the quantity: letter f will indicate propagation in the fluid and letters P and S propagation in the solid with longitudinal or transverse polarization, respectively. For example, a quantity with subscript ff is associated with a path of two segments in the fluid; a quantity with subscript $fPSf$ is associated with a path of four segments, the first and the last in the fluid, the two others in the solid.

The pressure at the receiver, in the Laplace–Fourier domain, is

$$\tilde{p} = \tilde{p}_D + \tilde{p}_R + \tilde{p}_{R1}, \tag{10}$$

where the expression of each term is given below.

Direct wave (D): The pressure $\tilde{p}_D$ in the transform domain due to the direct wave is given by Eq. (9)

$$\tilde{p}_D = \frac{\rho_f \hat{\phi}_V}{2\gamma_f} \exp(-s\gamma_f(h_s - h_r)). \tag{11}$$

Reflected wave (R): The pressure $\tilde{p}_R$ in the transform domain due to the wave reflected on the fluid–solid interface is obtained by construction with the generalized ray theory: the expression for the direct wave Eq. (11) is multiplied by the reflection coefficient at the fluid–solid interface R_{ff} and a phase term is added

$$\tilde{p}_R = \frac{\rho_f \hat{\phi}_V}{2\gamma_f} R_{ff} \exp(-s\gamma_f(h_s + h_r)), \tag{12}$$

where R_{ff} is obtained from the interface conditions Eq. (5),

$$R_{ff} = \frac{4\mu\gamma_f \Delta_R - \gamma_P \rho_f s_S^2}{4\mu\gamma_f \Delta_R + \gamma_P \rho_f s_S^2},$$

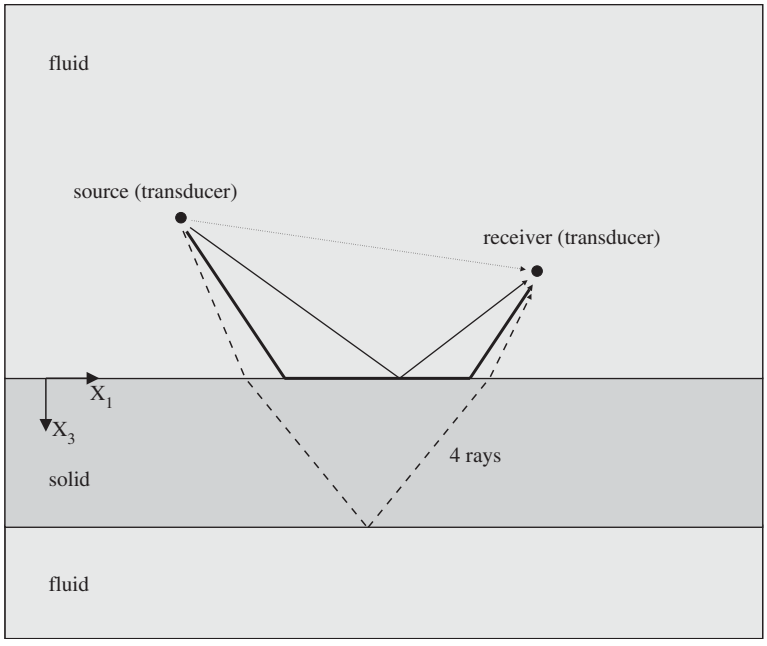

Fig. 3. Wave paths. The four types of wave paths are sketched: ... direct wave (D); — (thin line) reflected waves, except the head waves; — (thick line) head waves (R); - - - waves reflected at the bottom surface ($R1$).

where $\gamma_P = (s_P^2 - \xi^2)^{1/2}$, $\gamma_S = (s_S^2 - \xi^2)^{1/2}$, $\chi = 0.5s_S^2 - \xi^2$ and $\Delta_R = \gamma_P\gamma_S\xi^2 + \chi^2$. For the derivations to follow, it is necessary to restrict the values of ξ to a single sheet of the Riemann surface corresponding to $\mathrm{Re}[\gamma_{P,S}] \geqslant 0$.

Waves reflected on the bottom surface ($R1$): The pressure $\tilde{p}_{R1}$ in the transform domain due to the waves reflected once on the bottom surface and transmitted back into the fluid is split into four contributions: $\tilde{p}_{R1} = \tilde{p}_{fPPf} + \tilde{p}_{fSPf} + \tilde{p}_{fPSf} + \tilde{p}_{fSSf}$, where the combinations of letters P and S indicate the polarization of the wave, before and after reflection on the bottom interface. Each of the four wave contributions is obtained by construction with the generalized ray theory: the expression for the direct wave Eq. (11) is multiplied by the appropriate transmission and reflection coefficients and a phase term is added. The wave amplitudes are given by

$$\begin{aligned}
\tilde{p}_{fPPf} &= \frac{\rho_f\hat{\phi}_V}{2\gamma_f} T_{fP}R_{PP}T_{Pf}\exp[-s(\gamma_f(h_s+h_r)+2\gamma_P h)],\\
\tilde{p}_{fSPf} &= \frac{\rho_f\hat{\phi}_V}{2\gamma_f} T_{fS}R_{SP}T_{Pf}\exp[-s(\gamma_f(h_s+h_r)+(\gamma_P+\gamma_S)h)],\\
\tilde{p}_{fPSf} &= \frac{\rho_f\hat{\phi}_V}{2\gamma_f} T_{fP}R_{PS}T_{Sf}\exp[-s(\gamma_f(h_s+h_r)+(\gamma_P+\gamma_S)h)],\\
\tilde{p}_{fSSf} &= \frac{\rho_f\hat{\phi}_V}{2\gamma_f} T_{fS}R_{SS}T_{Sf}\exp[-s(\gamma_f(h_s+h_r)+2\gamma_S h)],
\end{aligned} \tag{13}$$

where $T_{\alpha\beta}$ and $R_{\alpha\beta}$ ($\alpha, \beta = P, S$ or f) are coefficients of transmission at the fluid–solid interface and coefficients of reflection at the bottom surface, respectively; subscript α indicates the polarization of the wave incident on the interface and β of the wave transmitted or reflected; for example, T_{fP} is the transmission coefficient of a wave in the fluid transmitted in the solid as a P-wave and R_{PS} is the reflection coefficient for an incident P-wave converted into a S-wave after reflection on the bottom surface. These coefficients are obtained from the interface conditions Eq. (5),

$$\begin{aligned}
T_{fP} &= \frac{4s_P\gamma_f\chi}{4\gamma_f\mu\Delta_R + \gamma_P\rho_f s_S^2},\\
T_{fS} &= \frac{4s_S\gamma_P\gamma_f\xi}{4\gamma_f\mu\Delta_R + \gamma_P\rho_f s_S^2}\\
T_{Pf} &= \frac{4\gamma_P\mu c_P\rho_f\chi s_S^2}{4\gamma_f\mu\Delta_R + \gamma_P\rho_f s_S^2}\\
T_{Sf} &= -\frac{4\gamma_P\gamma_S c_S\xi\mu\rho_f s_S^2}{4\gamma_f\mu\Delta_R + \gamma_P\rho_f s_S^2},
\end{aligned} \tag{14}$$

$$\begin{aligned}
R_{PP} &= \frac{4\gamma_f\mu(\gamma_P\gamma_S\xi^2 - \chi^2) + \gamma_P\rho_f s_S^2}{4\gamma_f\mu\Delta_R + \gamma_P\rho_f s_S^2},\\
R_{PS} &= \frac{8c_P s_S\gamma_P\gamma_f\xi\mu\chi}{4\gamma_f\mu\Delta_R + \gamma_P\rho_f s_S^2},\\
R_{SP} &= -\frac{8c_S s_P\gamma_S\gamma_f\xi\mu\chi}{4\gamma_f\mu\Delta_R + \gamma_P\rho_f s_S^2},\\
R_{SS} &= \frac{4\gamma_f\mu(\gamma_P\gamma_S\xi^2 - \chi^2) - \gamma_P\rho_f s_S^2}{4\gamma_f\mu\Delta_R + \gamma_P\rho_f s_S^2}.
\end{aligned} \tag{15}$$

4. Solution in the space-time domain

The Cagniard–de Hoop method [10,11] is used to invert the transform domain solutions. The method is applied to each generalized ray contribution, that is, to each term appearing in Eqs. (11)–(13). It is not the

purpose of this paper to give a complete account of the method of solution—the Cagniard–de Hoop technique has been presented in great details elsewhere [13,19]. For the sake of clarity, the method is briefly presented for the contribution (R); only the final solutions are given for (D) and ($R1$).

4.1. Body waves and lateral waves

In Fig. 3, the reflected wave (R) is represented with two different paths which correspond to two wave contributions—but a single generalized ray. In the transform domain, the two contributions are contained in essence in Eq. (12). As the Cagniard–de Hoop method is used to invert the transform-domain solution, the two contributions are separated. One contribution is the "body wave": the wave reflected at the fluid–solid interface with an arrival time predicted by the laws of geometrical acoustics. The other contribution is the "lateral waves" (or "head waves"): waves associated with energy propagated in the solid, close to interface, at the speed of P- or S-waves and refracted back in the fluid. Any interaction of waves with an interface may give rise to lateral wave contributions under certain conditions on the material properties. One important feature of lateral waves is that they arrive at a receiver before the associated body wave. A theoretical presentation of lateral wave phenomena may be found in the monograph by Brekhovskikh [20] (p. 260).

4.2. Contribution of the reflected wave (R)

Application of the inverse Fourier transform to Eq. (12) yields the Laplace transform of the reflected wave contribution

$$\hat{p}_R = \frac{-\mathrm{i}s\rho_f \hat{\phi}_V}{4\pi} \int_{-i\infty}^{i\infty} \frac{1}{\gamma_f} R_{ff} \exp[-s(\gamma_f(h_s + h_r) + \xi x_1)] \,\mathrm{d}\xi. \tag{16}$$

In the subsequent operations, the integration contour (imaginary axis) will be changed so that the integral in Eq. (16) takes the form of a forward Laplace transform. Once this is achieved, the inverse Laplace transform is obtained by inspection. The change of integration contour is performed *via* the change of variable

$$\tau = \gamma_f(h_s + h_r) + \xi x_1, \tag{17}$$

where τ is real and positive. The solution of Eq. (17) for ξ is

$$\xi = \frac{\tau x_1}{r^2} \pm i \frac{h_r + h_s}{r^2} \sqrt{\tau^2 - t_{ff}^2}, \tag{18}$$

where $r^2 = (h_r + h_s)^2 + x_1^2$ and $t_{ff} = s_f r$ is the arrival time of the body wave. The new integration contour, with τ as a parameter, is Eq. (18).

Due to the conditions specified above for the radicals γ_f, γ_P and γ_S, analytic continuation of the integrand can only take place in a ξ-plane cut along the real axis: $]-\infty, s_f]$, $]-\infty, s_S]$, $]-\infty, s_P]$, $[s_P, +\infty[$, $[s_S, +\infty[$ and $[s_f, +\infty[$.

The change of contour integration is performed based on Cauchy's theorem, applied in the right half of the complex plane. The closed contour for the application of Cauchy's theorem is made of: (i) the original integration contour on the imaginary axis (see Eq. (16)); (ii) two circular arcs centered on the origin and with infinite radius which contributions vanish (Jordan's lemma); (iii) the contour defined by Eq. (18).

For $0 < \tau < t_{ff}$, the Cagniard–de Hoop contour runs along the real axis. The contour becomes complex for $\tau > t_{ff}$; this transition occurs at $\xi(t_{ff})$. For the material configurations considered in this paper, the condition $s_P < s_S < s_f$ is always satisfied, hence s_P is always the leftmost branch point. Furthermore, for the cases considered in this paper, we always have $\xi(t_{ff}) < s_S$. In those cases where $s_P < \xi(t_{ff}) < s_S$, the Cagniard–de Hoop contour has a part along a branch cut, from $\xi = s_P$ to $\xi(t_{ff})$. This integration along the cut gives rise to a contribution, in the space-time domain, which corresponds to a lateral wave; as expected, this contribution arrives at the receiver before the body wave. The condition $s_P < \xi(t_{ff})$ corresponds to the classical condition for the occurrence of lateral waves (critical angle) and taking $\xi = s_P$ in Eq. (17) yields the arrival time t_l of the lateral wave contribution.

The final solution for the contribution of the reflected wave in the space-time domain is

$$\text{if } \xi(t_{ff}) < s_P,\ p_R = \begin{cases} 0, & t < t_{ff}, \\ \partial_t \phi_V * \frac{-\rho_f}{2\pi\sqrt{t^2 - t_{ff}^2}} \mathrm{Re}[R_{ff}(\xi)], & t > t_{ff}, \end{cases}$$

$$\text{if } \xi(t_{ff}) > s_P,\ p_R = \begin{cases} 0, & t < t_l, \\ \partial_t \phi_V * \frac{\rho_f}{2\pi\sqrt{t_{ff}^2 - t^2}} \mathrm{Im}[R_{ff}(\xi)], & t_l < t < t_{ff}, \\ \partial_t \phi_V * \frac{-\rho_f}{2\pi\sqrt{t^2 - t_{ff}^2}} \mathrm{Re}[R_{ff}(\xi)], & t > t_{ff}. \end{cases} \tag{19}$$

where Im[.] denotes the imaginary part of the quantity between brackets and the time convolution is denoted by $*$. In Ref. [21], de Hoop and van der Hijden investigated, in the general case, the reflection at a fluid–solid interface with the Cagniard–de Hoop method. They presented a solution similar to Eq. (19), although in a slightly different form due to a difference in the formulation of the basic equations.

4.3. Contribution of the direct wave (D)

The amplitude in the space-time domain of the direct wave is derived from Eq. (11) with the Cagniard–de Hoop method, the final solution is

$$p_D = \begin{cases} 0, & t < t_D, \\ \partial_t \phi_V * \frac{-\rho_f}{2\pi\sqrt{t^2 - t_D^2}} & t > t_D, \end{cases} \tag{20}$$

where $t_D = s_f \sqrt{x_1^2 + (h_s - h_r)^2}$ is the arrival time of the direct wave.

4.4. Contributions of the waves reflected on the bottom surface (R1)

The amplitude of the four waves that contribute to p_{R1} are derived from Eqs. (13) with the Cagniard–de Hoop method. In the general case, these amplitudes do not have an explicit analytic expression because the Cagniard–de Hoop contours are not explicit.

The four amplitudes in the space-time domain are

$$p_{fPPf} = \begin{cases} 0, & t < t_{PP}, \\ \partial_t \phi_V * \frac{1}{4\pi} \mathrm{Im}\left[\frac{\rho_f}{\gamma_f} T_{fP} R_{PP} T_{Pf} \partial_t \xi\right], & t > t_{PP}, \end{cases}$$

$$p_{fPSf} = \begin{cases} 0, & t < t_{PS}, \\ \partial_t \phi_V * \frac{1}{4\pi} \mathrm{Im}\left[\frac{\rho_f}{\gamma_f} T_{fP} R_{PS} T_{Sf} \partial_t \xi\right], & t > t_{PS}, \end{cases}$$

$$p_{fSPf} = \begin{cases} 0, & t < t_{SP}, \\ \partial_t \phi_V * \frac{1}{4\pi} \mathrm{Im}\left[\frac{\rho_f}{\gamma_f} T_{fS} R_{SP} T_{Pf} \partial_t \xi\right], & t > t_{SP}, \end{cases}$$

$$p_{fSSf} = \begin{cases} 0, & t < \min(t_l, t_{SS}), \\ \partial_t \phi_V * \frac{1}{4\pi} \mathrm{Im}\left[\frac{\rho_f}{\gamma_f} T_{fS} R_{SS} T_{Sf} \partial_t \xi\right] & t > \min(t_l, t_{SS}), \end{cases} \tag{21}$$

where $t_{\alpha\beta}$ $(\alpha\beta = P, S)$ is the arrival time of the body wave associated with a given ray. In each of these expressions, $\xi(t)$ is solution of an equation similar to Eq. (17) deduced from the phase term of the particular ray (in the exponential terms in Eqs. (13)).

5. Numerical calculations

The steps of the Cagniard–de Hoop method described in this paper have been implemented in the symbolic and numerical software Mathematica. The expression of the generalized rays are generated upon combining the different factors; the reflection and transmission coefficients are derived automatically from the boundary conditions.

The Cagniard–de Hoop contours for the contributions ($R1$) are calculated with the standard Mathematica iterative method for solving equations. Convolutions are performed with the standard Mathematica procedure for numerical integration; the procedure must take care of the discontinuities at the arrival times of the direct wave and the reflected waves.

A finite element model of the ATT, corresponding to the configuration represented in Fig. 2 has been developed in parallel to the present work. The solutions obtained with the Cagniard–de Hoop method have been compared with the finite element solutions; when the finite element mesh is fine, the plots of the two solutions are indistinguishable

Material properties: The fluid is modeled as water: $\rho_f = 1000\,\mathrm{kg\,m^{-3}}$ and $c_f = 1490\,\mathrm{m\,s^{-1}}$. Except in Section 6.2.2, the following values are used for the mass density of bone $\rho_s = 1850\,\mathrm{kg\,m^{-3}}$, velocity of transverse waves $c_S = 1800\,\mathrm{m\,s^{-1}}$ and velocity of longitudinal waves $c_P = 4000\,\mathrm{m\,s^{-1}}$ in bone [7,22].

Receiver locations: Responses are calculated for various receiver locations. Receivers P1, P2 and P3 are located at $(x_1, x_3) = (20, -2), (50, -2)$ and $(80, -2)$ (dimensions in mm), respectively (source-receiver distance of 20, 50 and 80 cm, respectively). In Section 6.1.2, the close-field wave phenomena are addressed: responses are calculated at receivers placed at less than 2 cm from the source. Note that in the devices based on the ATT, the physical distance between source and receiver is 10–30 mm [9].

6. Results

6.1. Green's functions

6.1.1. Reflection at the fluid–solid interface (R)

The Green's functions at receivers P1–P3, calculated according to Eq. (19), are shown in Fig. 4. Four instants, each associated with a certain mode of propagation of the energy are marked with arrows on the figure:

- The lateral P-wave contribution arrives at t_l^P. This contribution corresponds to energy propagated in the fluid and, in the solid, close to the interface, with longitudinal polarization. The amplitude of the lateral P-wave returns to zero at a time t_e defined by [21]

$$t_e = \frac{x_1}{\sqrt{2}c_S} + \sqrt{s_f^2 - 0.5s_S^2}(h_r + h_s). \tag{22}$$

  Note that this time does not depend on the longitudinal wave speed in the solid;
- The lateral S-wave contribution arrives at t_l^S. This contribution corresponds to energy propagated in the fluid and, in the solid, close to the interface, with transverse polarization;
- The contribution of the body wave reflected at the fluid-solid interface, with arrival time t_{ff}. This contribution corresponds to energy propagated in the fluid only. Note that the amplitude of the Green's function is infinite at this arrival time.
- The contribution due to a pole in the reflection coefficient R_{ff} is associated with the propagation of a Scholte interface wave at the fluid-solid interface. Unless a receiver is placed *on* the interface, this contribution does not have an arrival time in the usual sense of the word. However, the speed of the Scholte wave c_{Sch} is defined as $1/\xi_{\mathrm{Sch}}$ where ξ_{Sch} is solution of $R_{ff} = 0$; an "arrival time" for the Scholte wave contribution can be defined as $t_{\mathrm{Sch}} = x_1/c_{\mathrm{Sch}}$ [21].

6.1.2. Close field effects

The minimum wavelengths in the fluid (λ_f) and the solid layer ($\lambda^{P,S}$) are, for the 1 MHz pulse and the material properties given above, $\lambda_f = 1.49\,\mathrm{mm}$, $\lambda^P = 4\,\mathrm{mm}$ and $\lambda^S = 1.8\,\mathrm{mm}$. Considering the typical

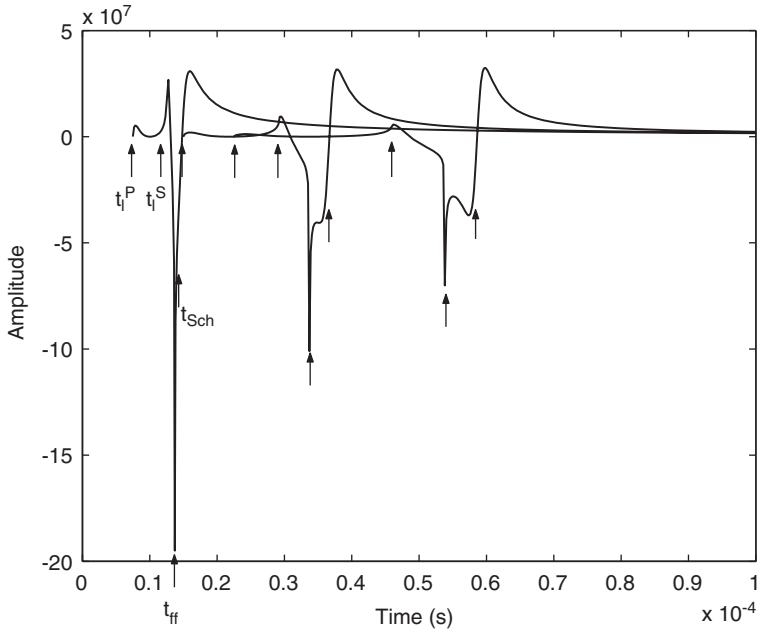

Fig. 4. Green's function for the reflected wave contribution (R) at receivers P1–P3. Four arrows per curve indicate the arrival times (t_l^P, t_l^S, t_{ff} and t_{Sch}) of four waves (lateral P-wave, lateral S-wave, reflected body wave and Scholte wave, respectively).

source–receiver distances of devices based on the ATT (1–3 cm), near field effects are expected to be involved in ATT experiments [7].

At present, the evaluation of bone mechanical properties with the ATT are based on the first signal arriving at the receiver. In many cases, this signal is due to the lateral P-wave. In Fig. 5, the part of the Green's functions corresponding to the lateral P-wave contribution is presented for receivers at $2 \leqslant x_1 \leqslant 20$ and $h_r = 2$ (dimensions in mm). Each Green's function is plotted for $t_l^P < t < t_e$, according to Eq. (19). In the near field, the Green's functions undergo strong amplitude decay with and increase of the "duration" of the lateral P-wave contribution with the source–receiver distance.

6.1.3. Finite cortical thickness

The Green's functions presented in Sections 6.1.1 and 6.1.2 correspond to the reflection of a wave at the interface between a semi-infinite fluid medium and a semi-infinite solid medium, i.e., corresponding to an infinite cortical thickness. Due to the finite thickness of the cortical layer, waves are reflected on the bottom surface and bring energy back to the receiver placed in the fluid. In Fig. 6, Green's functions of contributions (R) and ($R1$) are shown together. Note that the plots corresponding to the contributions (R1) do not correspond to a physical response, in particular they start from non-zero amplitude values. At short times, the corresponding physical signal is the sum of the contributions (R) and (R1).

Fig. 7 shows the Green's functions of the contributions (R) and ($R1$), for various values of the cortical thickness, a short time after the arrival of first wave.

With the two wave contributions (R) and ($R1$) at hand, one can infer the way they are likely to interfere in an ATT experiment, depending on the value of h. In particular, the influence of the arrival time and the shape of ($R1$) can be estimated. Note in Fig. 7 that there is an important change in the shape of the contribution ($R1$) in the interval $2 < h < 5$ (in mm).

Note that in a given time window, the exact Green's function of the problem must include the contributions of all the rays whose arrival times fall in the time window; hence summing the amplitudes of (R) and ($R1$) is not, in the general case, the exact response.

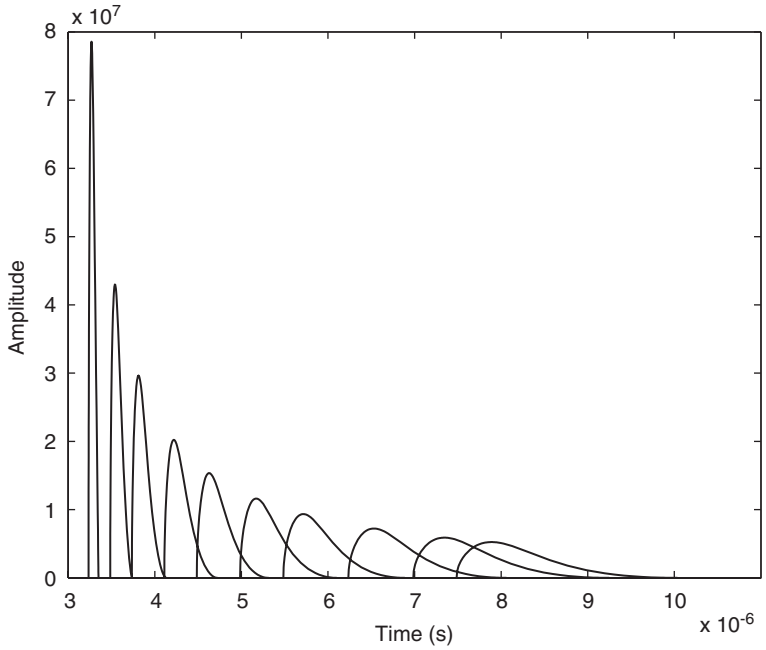

Fig. 5. Green's function for the lateral P-wave in near field. Receivers are placed at $x_3 = -0.002\,\text{mm}$ and $x_1 = 3, 4, 5, 6.5, 8, 10, 12, 15, 18, 20\,\text{mm}$.

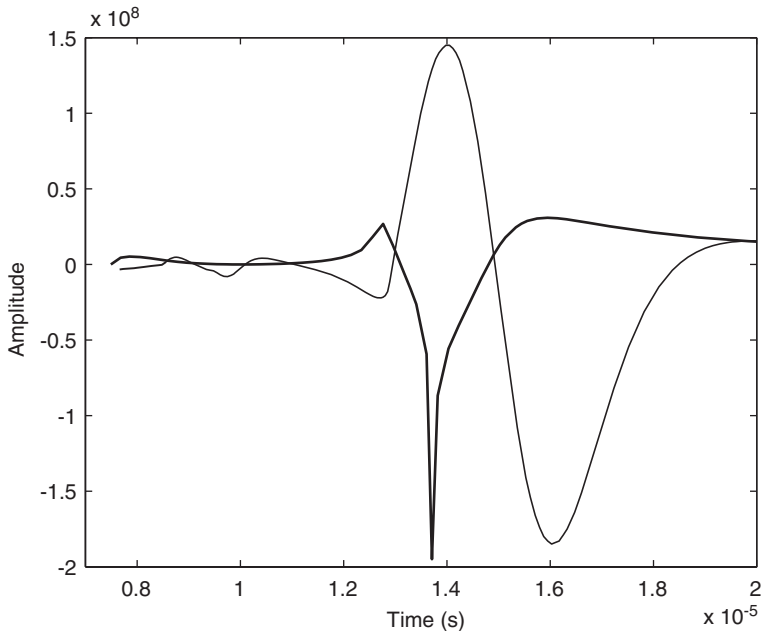

Fig. 6. Green's functions of the contributions (R) (thick line) and ($R1$) (thin line) at receiver P1, with $h = 2\,\text{mm}$.

6.2. Acoustic pressure

The simulation of an axial transmission experiment consists in calculating the acoustic pressure to a given excitation produced by a ultrasonic transducer. With the Cagniard–de Hoop method, the acoustic pressure is

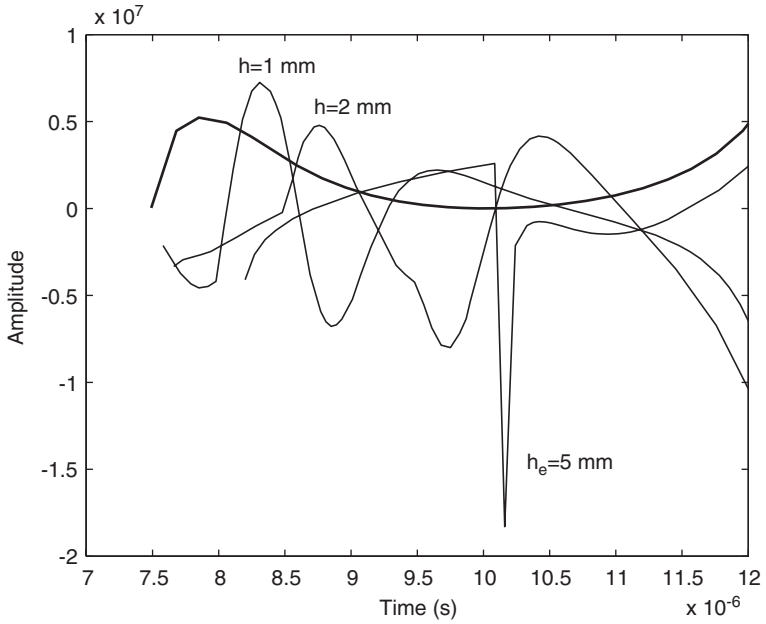

Fig. 7. Green's functions of contribution (R) corresponding to the lateral P-wave part (thick line) and of ($R1$) for three values of the cortical thickness h (thin line), indicated on the figure in mm. Responses calculated at receiver P1.

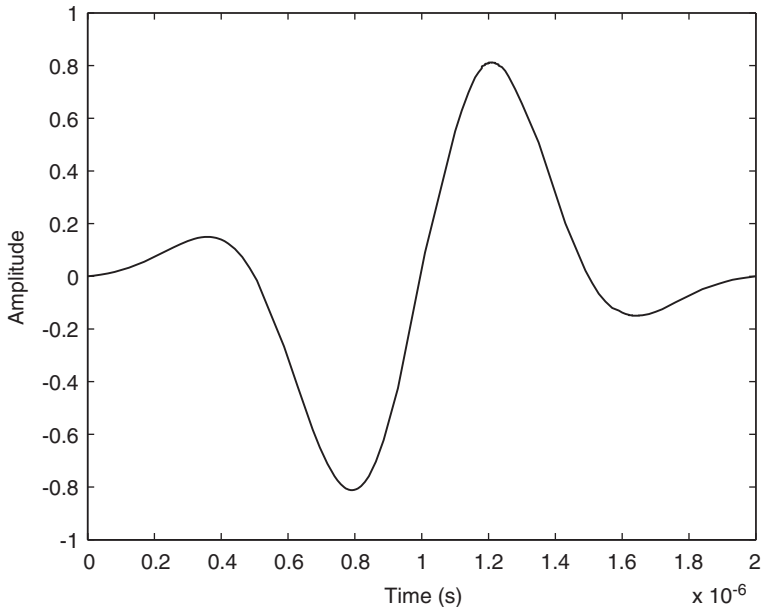

Fig. 8. Pressure source pulse $\partial_t \phi_V(t)$ with 1 MHz center frequency.

obtained by convolution of Green's functions with a function $\partial_t \phi_V(t)$ which describes the source history. The shape of the pressure source pulse used in the computations is shown in Fig. 8.

Three pulses were used in the present study, referred to by their center frequency: 0.5, 1, and 2 MHz with durations 4, 2 and 1 μs, respectively.

6.2.1. Convolved responses

In Fig. 9, responses at P1–P3 are plotted for the three pulses at 0.5, 1, and 2 MHz. The influence of the pulse center frequency on the relative amplitudes of the waves (lateral waves, Scholte wave, etc.) is observed.

For the evaluation of bone mechanical properties, the signal of the direct wave (D) (which has not interacted with bone) is useless. With the Cagniard–de Hoop method, the contribution of (D) can be isolated from the rest of the response. An illustration of this is presented in Fig. 10: the acoustic pressure for a 1 MHz pulse at receivers P1–P3 are shown for (i) (D) only and (ii) the sum of $(D)+(R)$. At P1–P3, it is manifest that the contribution of the direct wave is localized in time around the arrival time of the reflected body wave, and that (D) does not interfere with the lateral wave contributions.

6.2.2. Influence of the material parameters

In this subsection, we investigate the sensitivity of the near-field acoustic pressure due to lateral P-wave contribution to the material parameters; contributions of (D) and ($R1$) are ignored in this section.

The effect of varying the longitudinal wave speed is addressed in Fig. 11. The arrival time of the lateral wave is clearly dependent on the value of c_P: it corresponds to energy which has travelled at the longitudinal wave speed in the solid. The evolutions of the amplitudes of the various maxima of the signal are not linear with c_P: the three local maxima take their largest value for $c_P = 3650\,\mathrm{m\,s^{-1}}$.

According to the definition of t_e in Eq. (22) for the Green's function of the reflected wave, the various plot in Fig. 11 coincide some time after the arrival of the lateral wave: this is because t_e does not depend on c_P.

Other calculations (results not shown) indicated that the influence on the acoustic pressure of the bone density of mass ($1600 < \rho_s < 2000\,\mathrm{kg\,m^{-3}}$), all other parameters being kept constant ($c_P = 4000\,\mathrm{m\,s^{-1}}$ and $c_S = 1800\,\mathrm{m\,s^{-1}}$), is small. The amplitude variations of the lateral P-wave part of the signal, for the 1 and 2 MHz pulse, are 15% and 10%, respectively, in near field.

7. Discussion and conclusion

Modeling the axial transmission experiment (Figs. 1 and 2) is a challenging task with several aspects that can be addressed separately in preliminary studies. One aspect of the problem is to model the ultrasound

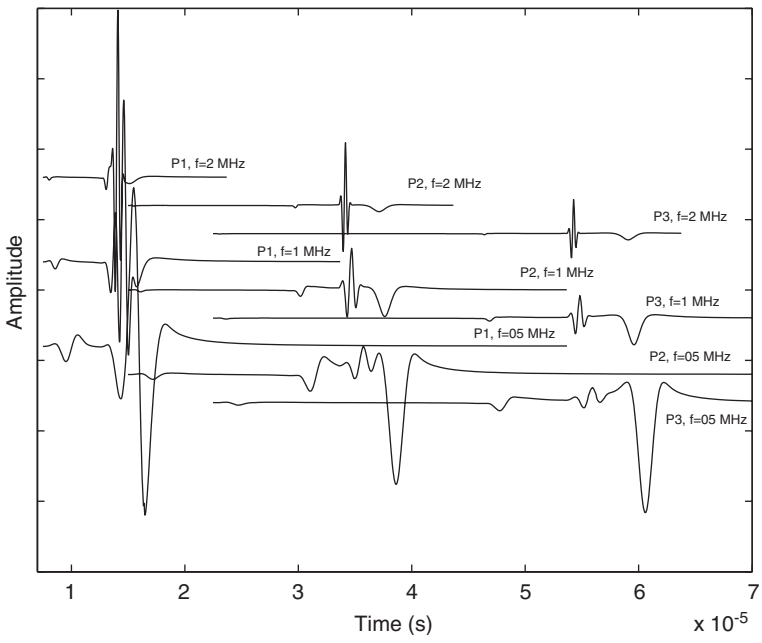

Fig. 9. Convolved responses at P1–P3 for the sum of the contributions of the direct (D) and reflected waves (R).

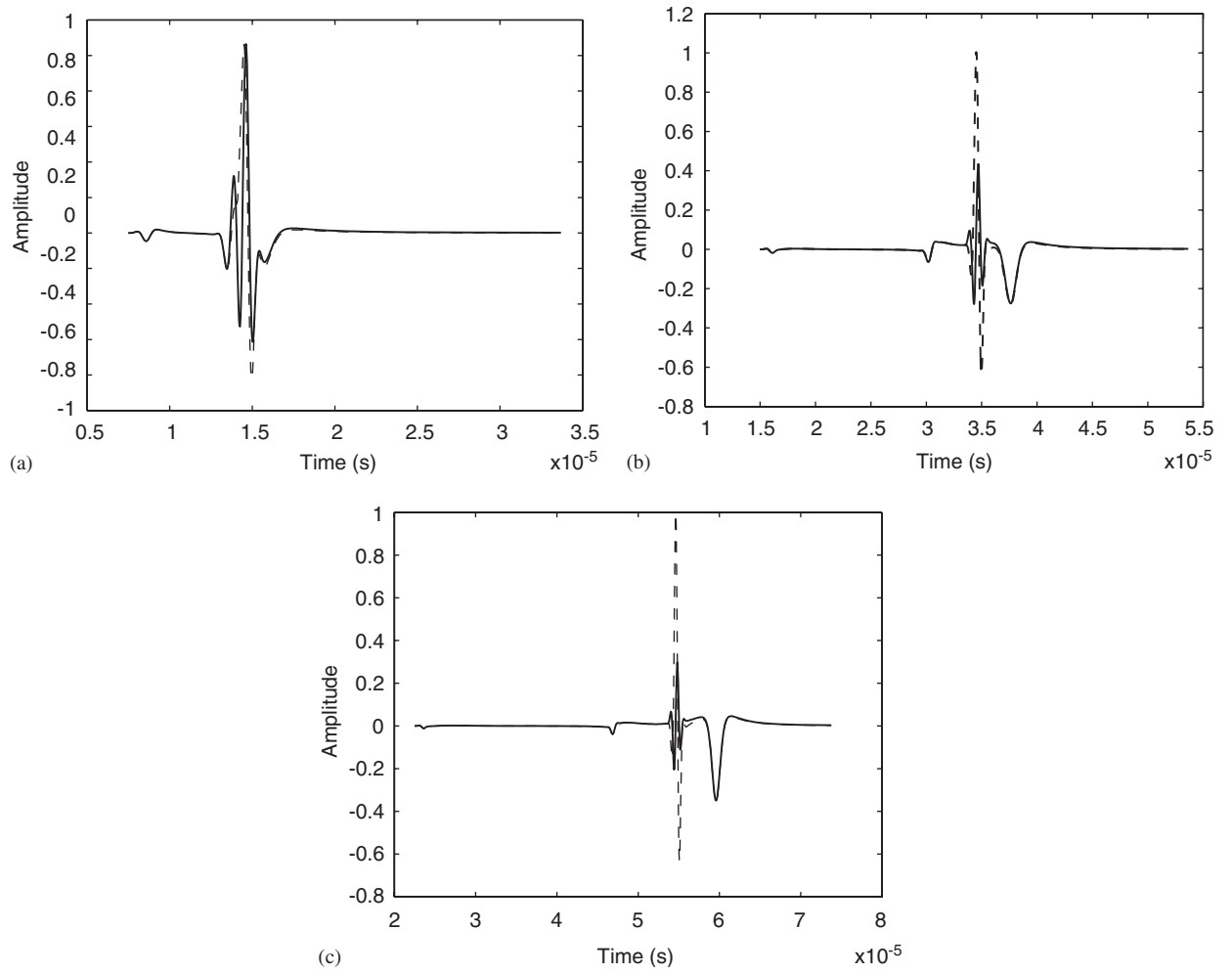

Fig. 10. Acoustic pressure for a 1 MHz pulse. The continuous line corresponds to the sum of (D) and (R); the discontinuous line corresponds to the contribution of (D) alone. (a) Response at P1. (b) Response at P2. (c) Response at P3.

device and the interaction between the transducer and the coupling gel. Another is to model the interaction of waves with bone and soft tissues. The present study is a contribution to the latter problem.

Several simplifications of the physical problem have been made. The model was derived based on the following considerations: (1) The devices based on the ATT generate pulses at a center frequency between 0.5 and 2 MHz; with these frequencies bone tissue can be modeled as a homogeneous medium. (2) Cortical bone is transversely isotropic [1], the wave speeds in the transverse direction (direction $\mathbf{x}_3$) are about 50% those in the longitudinal direction (direction $\mathbf{x}_1$); in the present work, the wave speeds in the solid correspond to the wave speeds in the longitudinal direction of the transversely isotropic cortical layer. It can be inferred from the results presented that, if taken into account in the model, the main effect of anisotropy would be to increase the arrival time of waves reflected on the bottom surface ($R1$). (3) With the 2D model used, the curvature of the bone layer in a direction normal to $\mathbf{x}_3$ ignored. It has been shown in Ref. [9] that the effect of the curvature on the response is small and that 2D modeling is relevant. (4) Soft tissues were modeled by an ideal fluid medium, thus disregarding the propagation of shear waves in these tissues. This is partially based on the assumption that shear waves are highly attenuated in soft biological media. More importantly, the ATT experiment consists in observing wave phenomena in a short time window after the arrival of the first signal. The low velocity of shear waves in soft tissues prevents the arrival of the associated contributions in the time window of interest.

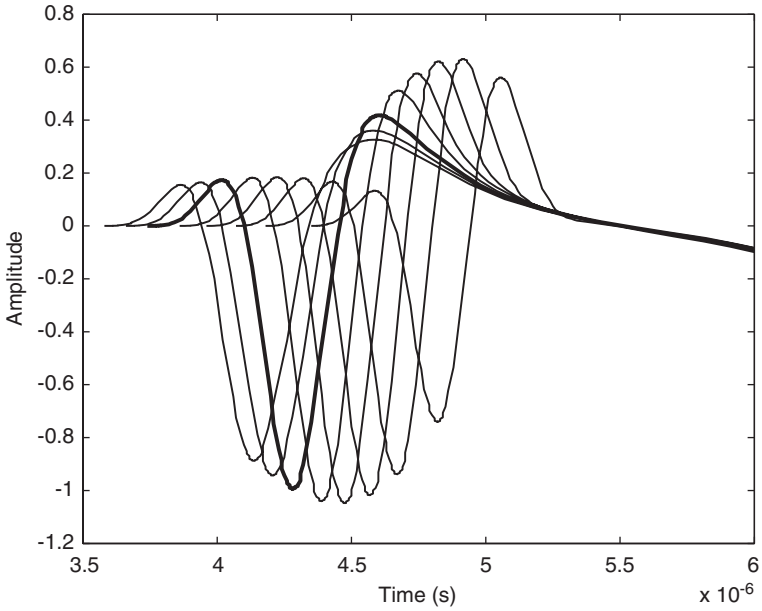

Fig. 11. Influence of the value of c_P on the lateral wave acoustic pressure (2 MHz excitation pulse), at point $x_1 = 10\,\text{mm}$, $h_s = 1\,\text{mm}$. The thick curve corresponds to $\rho_s = 1850\,\text{kg m}^{-3}$, $c_P = 4000\,\text{m s}^{-1}$ and $c_S = 1800\,\text{m s}^{-1}$; the thin lines correspond to $c_P = 4300, 4150, 3800, 3650, 3500, 3350, 3150\,\text{m s}^{-1}$, from left to right, all other parameters are kept constant.

The results presented in Section 6 have been selected so as to highlight the potential of the method for the understanding of wave phenomena involved in the ATT experiment. Future development of ATT-based devices for the evaluation of bone mechanical properties should benefit from a deep understanding of these phenomena which are complex and numerous.

Green's functions (Fig. 4) and convolved responses (Fig. 9) plotted for points P1–P3 demonstrate some typical features of wave reflection on a fluid–solid interface: arrival of lateral waves, followed by the body wave and the Scholte wave. The influence of summing the direct wave contribution to the reflected wave contribution can be inferred from plots such as Fig. 10.

The pulse duration (or center frequency) has a direct influence on the relative amplitudes of the wave contributions. Fig. 9 shows that the lower frequency pulse used (0.5 MHz center frequency) yields a larger amplitude of the lateral *P*-wave (relative to other wave contributions *at the same frequency*).

Part of the work has focused on responses at receivers "close" to the source of waves (near field) and in a short time window beginning at the arrival time of the lateral *P*-wave and ending 2–4 μs later. This is the part of the signal that is used at present in the ATT: the time of flight of a wave (between the source and the receiver) is estimated based on the first arriving signal. Signal processing techniques used for the determination of the arrival time are sensitive to the temporal shape of first arriving signal [7]. Results indicate that the shape of the lateral *P*-wave contribution changes rapidly with the source–receiver distance (Fig. 5) and that the amplitude of contribution ($R1$) is of the same order of magnitude as that of the lateral *P*-wave and may strongly interfere, for realistic cortical thicknesses (Figs. 6 and 7).

In the present study, only the waves reflected once on the bottom layer have been taken into account. As a consequence, responses calculated are exact only in a short time window after the first arriving signal. Although there is no formal limitation on the number of generalized rays that can be calculated with Cagniard–de Hoop, there is, in practice, a limitation because the time required to obtain a numerical solution increases with the number of rays. Furthermore, when the response is the sum of many rays, it is often not relevant to analyse their contribution separately. Hence the method is not suited to low frequency analyses (long time of observation); its use should be limited to the analysis of responses including less than about ten reflections on the bottom surface. On the other hand, it is well-known that bone tissue is a highly attenuating

medium. Accordingly, it is expected that waves reflected on the bottom surface have smaller amplitudes than predicted with the model that does not take attenuation into account. Some complex phenomena induced by multiple wave reflections on the bottom layer have been addressed in Ref. [7] with the help of the finite difference method.

This paper describes a method to derive Green's functions in a model of the ATT. The convolution of a Green's functions with a source signal yields a response in terms of acoustic pressure. The method is based on the generalized ray theory and the Cagniard–de Hoop technique. With the Green's functions, the interaction of waves with the cortical layer can be analyzed independent of a pulse duration or specific frequency. The method also enables one to perform a time domain analysis of each wave contributions separately, even if they are superimposed in time; this is not possible with purely numerical methods.

Theoretical developments and physical responses have been presented for an isotropic layer; the investigation of wave reflection on a transversely isotropic cortical bone plate should now be conducted. The use of the Cagniard–de Hoop method is only one step towards an efficient modeling of the ATT experiment. Numerical methods of solution based on finite difference schemes are currently developed to take into a account the complex geometry of bone and surrounding tissues. Qualitative agreement of in vitro and simulated signals have been observed [9].

References

[1] S.C. Cowin, *Bone Mechanics Handbook*, second ed., CRC Press, Boca Raton, FL, 2001.

[2] R. Rizzoli, Diagnosis of osteoporosis; what should we be able to measure *in vivo*? in: *16th International Bone Densitometry Workshop*, Annecy, France, 2004.

[3] A.J. Foldes, A. Rimon, D.D. Keinan, M.M. Popovtzer, Quantitative ultrasound of the tibia: a novel approach for assessment of bone status, *Bone* 17 (1995) 363–367.

[4] G. Lowet, G. Van der Perre, Ultrasound velocity measurements in long bones: measurement method and simulation of ultrasound wave propagation, *Journal of Biomechanics* 29 (1996) 1255–1262.

[5] C.F. Njeh, I. Saeed, M. Grigorian, D.L. Kendler, B. Fan, J. Shepherd, M. McClung, W.M. Drake, H.K. Genant, Assessment of bone status using speed of sound at multiple anatomical sites, *Ultrasound in Medicine and Biology* 27 (2001) 1337–1345.

[6] E. Camus, M. Talmant, G. Berger, P. Laugier, Analysis of the axial transmission technique for the assessment of skeletal status, *Journal of the Acoustical Society of America* 108 (2000) 3058–3065.

[7] E. Bossy, M. Talmant, P. Laugier, Effect of bone cortical thickness on velocity measurements using ultrasonic axial transmission: A 2d simulation study, *Journal of the Acoustical Society of America* 112 (2002) 297–307.

[8] M. Muller. *In vivo* comparative study of three devices based on ultrasonic axial transmission, in: *16th International Bone Densitometry Workshop*, Annecy, France, 2004.

[9] E. Bossy. *Évaluation ultrasonore de l'os cortical par transmission axiale : modélisation et expérimentation* in vitro *et* in vivo, PhD Thesis, Université Pierre et Marie Curie, 2003.

[10] L. Cagniard. *Reflection and Refraction of Progressive Seismic Waves.* [*Traduction et révision par E.A. Flinn et C.H. Dix de L.* Cagniard *Réflexion et réfraction des ondes séismiques progressives. Gauthier-Villars*, *Paris*, 1939.], Mc-Graw Hill, New York, 1962.

[11] A.T. de Hoop, A modification of cagniard's method for solving seismic pulse problems, *Applied Scientific Research* 8 (1960) 349–356.

[12] Y. Pao, R. Gajewski, *The Generalized Ray Theory and Transient Response of Layered Elastic Solids*, Academic Press, New York and London, 1977.

[13] J.H.M.T. van der Hijden, *Propagation of Transient Elastic Waves in Stratified Anisotropic Media*, vol. 32. North Holland Series in Applied Mathematics and Mechanics, Elsevier Science Publishers, Amsterdam, 1987.

[14] A. Tadeu, J.M.P. António, Acoustic insulation of single panel walls provided by analytical expressions versus the mass law, *Journal of Sound and Vibration* 257 (3) (2002) 457–475.

[15] A.T. de Hoop, *Handbook of Radiation and Scattering of Waves: Acoustic Waves in Fluids, Elastic Waves in Solids, Electromagnetic Waves*, Academic Press, 1995.

[16] Q. Grimal, S. Naïli, A. Watzky, On the transmission of transient elastodynamic waves at a sliding contact interface; application to a weakly coupled bimaterial, *International Journal of Solids and Structures* 41 (2) (2004) 459–480.

[17] T.W. Spencer, The method of generalized reflection and transmission coefficients, *Geophysics* 25 (1960) 625–641.

[18] Q. Grimal, S. Naïli, A. Watzky, A method for calculating the axisymmetric response of a two-layered half-space under concentrated loading, *Journal of Sound and Vibration* 276 (3–5) (2004) 755–780.

[19] J.D. Achenbach, *Wave Propagation in Elastic Solids*, North-Holland, Amsterdam, 1973.

[20] L.M. Brekhovskikh, *Waves in Layered Media*, Academic Press, San Diego, 1973.

[21] A.T. de Hoop, J.H.M.T. van der Hijden, Generation of acoustic waves by an impulsive line source in a fluid/solid configuration with a plane boundary, *Journal of the Acoustical Society of America* 74 (1) (1983) 333–342.

[22] S. Bensamoun, M.-Ch. Ho Ba Tho, S. Luu, J.-M. Gherbezza, J.-F. de Belleval, Spatial distribution of acoustic and elastic properties of human femoral cortical bone, *Journal of Biomechanics* 37 (3) (2004) 503–510.